Available online at www.sciencedirect.com
ScienceDirect
Ceramics International 37 (2011) 333–340
CERAMICS INTERNATIONAL
www.elsevier.com/locate/ceramint

Synthesis, characterization and optical properties of $Zn_{1-x}Ti_xO$ nanoparticles prepared via a high-energy ball milling technique

Sumetha Suwanboon [a,*], Pongsaton Amornpitoksuk [b], Phuwadol Bangrak [c]

[a] Department of Materials Science and Technology, Faculty of Science, Prince of Songkla University, Hat Yai, Songkhla 90112, Thailand
[b] Department of Chemistry and Center for Innovation in Chemistry, Faculty of Science, Prince of Songkla University, Hat Yai, Songkhla 90112, Thailand
[c] School of Science, Walailak University, Nakhon Si Thammarat 80160, Thailand

Received 16 June 2010; received in revised form 19 July 2010; accepted 29 August 2010
Available online 29 September 2010

Abstract

$Zn_{1-x}Ti_xO$ ($x = 0$, 0.01, 0.03 and 0.05) nanoparticles were prepared by high-energy ball milling at 400 rpm. The milled powders were characterized by X-ray diffractometer (XRD) and the results exhibited that Ti-doped ZnO nanoparticles consisted of single phase with hexagonal structure when the mixtures of ZnO and TiO_2 powders were milled for 20 h. The crystallite size reduced as a function of the doping content and milling time from 1 to 10 h then increased after milling for 20 h and when the annealing temperature increased. The strain changed inversely to the crystallite size. A wider band-gap was obtained by increasing the doping content and annealing temperature because of a reduction in defect concentration. Both ZnO- and Ti-doped ZnO nanoparticles caused damage to *S. aureus*, *E. coli*, *P. mirabilis*, *S. typhi* and *P. aeruginosa*.

Key words : A. Powder; A. Milling; B. X-ray diffraction; D. ZnO

1. Introduction

Zinc oxide (ZnO) is an *n*-type semiconductor with a wide band-gap of about 3.2 eV and optical transparency in the visible region at room temperature [1]. This is because ZnO can absorb UV light through a process of electronic transition between the valence band and conduction band. Due to its unique properties, ZnO nanoparticles have been extensively used in various applications such as UV absorption [2], discoloration [3], optoelectronic devices [4] and antibacterial activity [5].

ZnO and metal-doped ZnO nanoparticles can be produced by two major approaches. In the first approach, ZnO nanoparticles can be prepared by chemical-based or solution-based methods such as sol–gel [6], precipitation [7] and a hydrothermal method [8]. In the second approach, ZnO nanoparticles can be prepared by mechanical milling techniques such as conventional ball milling [9] and high-energy ball milling [2]. All techniques above aim to reduce the crystallite and particle size and to produce ZnO particles with a narrow size distribution and regular particle shape. Due to the sophisticated processes of solution-based methods, the mechanical milling is an alternative route that can be used to prepare ZnO nanoparticles in a single step. Nowadays, high-energy ball milling has become a popular method to produce nanoparticles because this method involves strong ball impacts when colliding balls process a high value of kinetic energy [10]. Thus, more deformation, fracturing or cold welding of particles was produced and smaller particles were formed.

To date, a number of publications have dealt with the fabrication of ZnO and metal-doped ZnO nanoparticles by high-energy ball milling. Moballegh et al. [2] synthesized ZnO nanoparticles with a planetary mill for 9 h at 250 rpm. They reported that the absorbance of UV light increased with decreasing particle size and the particle size increased with an increasing calcination temperature. Vojisavljevic et al. [11] investigated the preparation of ZnO nanoparticles by milling at 400 rpm, the ball to powder ratio (BPR) was 40:1 and milling time was 30, 90 and 300 min. From this study, the XRD peak positions were shifted to a higher angle and the intrinsic defect concentration increased with increased milling time. Damonte et al. [12] investigated the structural and magnetic properties of $Zn_{1-x}Co_xO$ powders. Moreover, they also prepared

* Corresponding author. Tel.: +66 74 28 82 50; fax: +66 74 21 83 95.
E-mail address: ssuwanboon@yahoo.com (S. Suwanboon).

0272-8842/$36.00
doi:10.1016/j.ceramint.2010.08.039

$Zn_{1-x}Mg_xO$ and $Zn_{1-x}Cd_xO$ powders by milling for 1, 5, 10 and 20 h at 200 and 360 rpm and they found that the cation impurities produced a different signal in the PL spectra [13]. Dodd et al. [3] studied the photocatalytic activity of $Zn_{1-x}Co_xO$ and $Zn_{1-x}Mn_xO$ powders that had been milled for 6 h. The photocatalytic activity of $Zn_{1-x}Co_xO$ decreased with the doping content, but the activity of $Zn_{1-x}Mn_xO$ increased with the doping content up to 20 mol%. Marinkovic et al. [14] synthesized a nanocrystalline $ZnCr_2O_4$ spinel structure at room temperature using a planetary ball mill. In recent years, a few research groups have studied the preparation of nanocrystalline $Zn_{1-x}Ti_xO$ powders. Manik et al. [15,16] prepared $ZnTiO_3$ and Zn_2TiO_4 from ZnO and TiO_2 powders with a mol ratio of 1:1 and 2:1 when milling at 300 rpm for 5 min to 6 h and using a BPR = 35:1. Obradovic et al. [17–19] prepared Zn_2TiO_4 from ZnO and TiO_2 with a mol ratio of 2:1 under the following conditions: BPR = 40:1 or 20:1, speed = 400 rpm and milling time = 5, 15, 30, 90, 180 and 300 min. This investigation showed that mechanical activation led to an increase of contact necks and to the strengthening of the boundary regions of neighboring grains, thus influencing the final density and electrical properties of the samples.

To our knowledge, the preparation of $Zn_{1-x}Ti_xO$ ($x = 0.01$, 0.03 and 0.05) nanoparticles by high-energy ball milling as well as its enhancement of the optical band-gap as a function of annealing temperature and its antibacterial activity have not been reported. Therefore, this work could complete the missing information of Ti-doped ZnO nanoparticles prepared by this milling technique.

2. Experimental

The starting materials are ZnO and TiO_2 powders. ZnO was purchased from Fluka (Ananlytical grade), Japan and TiO_2 was purchased from Carlo Erba (Analytical grade), France. Powders were weighed to obtain mixtures of ZnO with 1, 3 and 5 mol% TiO_2. The milling was performed by a Pulverisette 7 FRITSCH planetary ball mill in air. Both vessel and balls used in this work are made from silicon nitride. The ball-to-powder weight ratio was 10:1. The milling speed was kept at 400 rpm and the mixtures were milled for 10 min, alternating with a stop for 5 min in order to prevent over heating and rapid engine wear. After the selected times (1, 5, 10 and 20 h), the milling was stopped to collect the samples.

The structural and phase formations were identified by an X-ray diffractometer (XRD, X'Pert MPD, PHILIPS). The morphological study was carried out by a scanning electron microscope (SEM, JSM-5800LV, JEOL) and the optical absorbance was measured by a UV–vis spectrophotometer (UV–vis 2450, Shimadzu).

Antibacterial tests were performed by an agar well diffusion assay using a Gram-positive bacterium *S. aureus* and Gram-negative bacteria *E. coli*, *P. mirabilis*, *S. typhi* and *P. aeruginosa* as indicator strains. The five species of bacteria were grown individually on nutrient agar plates at 37 °C for 16–18 h then resuspended in 0.85% sterile saline to produce a turbidity equivalent to the standard McFarland No. 0.5 with approximate 1.5×10^8 colony forming units/mL (CFU/mL). The suspension of tested bacteria was spread on Mueller-Hinton agar plates and left at room temperature for 5 min so as to allow the moisture from the inoculum to adsorb into the medium. Wells were punched in the agar with a sterile cock-borer of 9 mm diameter. The ZnO and $Zn_{0.95}Ti_{0.05}O$ (5 mg/mL) suspensions were filled directly into the wells of the agar plates previously inoculated with indicator bacteria. The agar plates were left at room temperature for 15 min and then incubated at 37 °C for 16 h in the dark and the diameters of any inhibition zones were finally measured in millimetres.

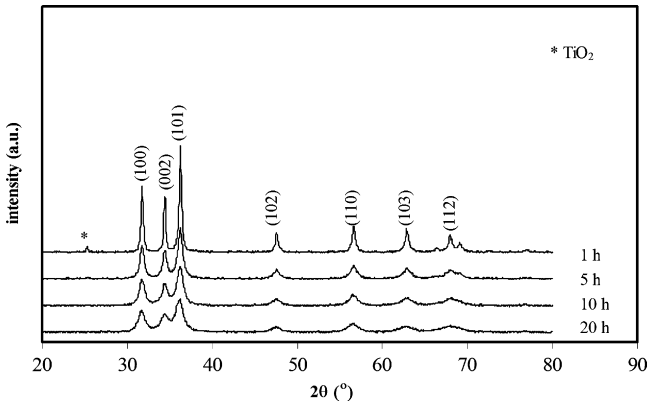

Fig. 1. XRD patterns of $Zn_{0.95}Ti_{0.05}O$ nanoparticles after different milling times.

3. Results and discussion

3.1. Effect of milling time

To seek a suitable milling time that will produce a homogeneous wurtzite structure, 0.0999 g TiO_2 ($x = 0.05$) powder was mixed with 2.0345 g ZnO powder and milled for 1, 5, 10 and 20 h. Any phase change was followed by the XRD technique and the results are presented in Fig. 1.

Taking into account the diffraction patterns of all samples in Fig. 1, TiO_2 powder with an anatase phase (a-TiO_2) was still observed after the mixture was milled for 10 h and this anatase

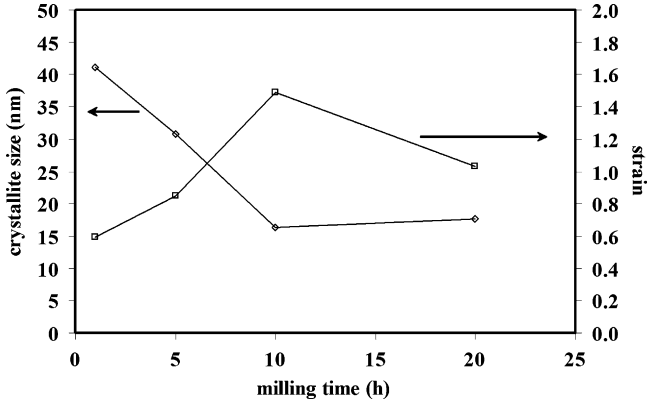

Fig. 2. Effect of milling time on the crystallite size and lattice strain of $Zn_{0.95}Ti_{0.05}O$ nanoparticles.

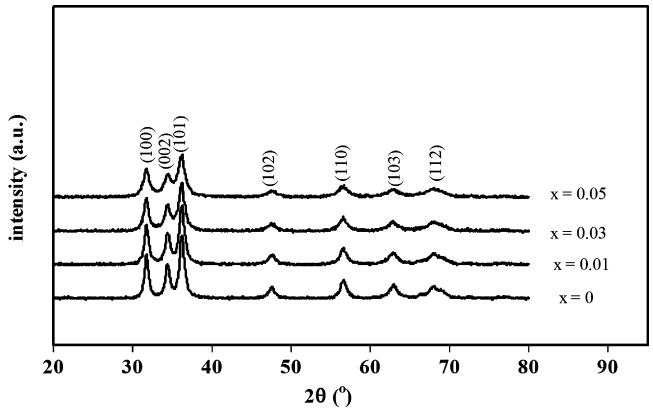

Fig. 3. XRD patterns of Ti-doped ZnO nanoparticles.

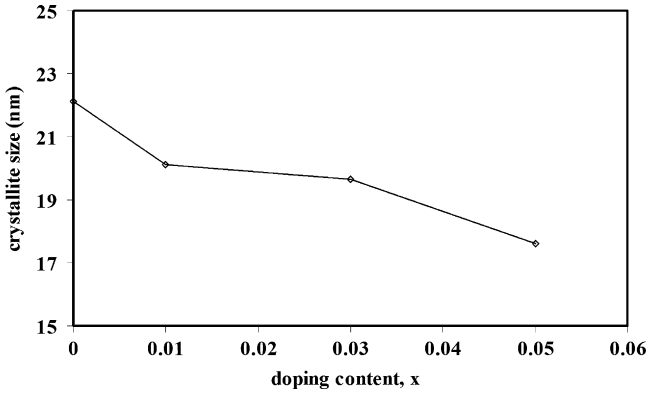

Fig. 4. Effect of the Ti doping content on crystallite size.

phase disappeared after milling for 20 h. The disappearance of the a-TiO_2 peak implied the existence of a solid solution. Thus, Ti-doped ZnO powder, with a hexagonal structure in accordance with the JCPDS of the ZnO standard (36-1451) was completely formed when the milling time was 20 h because of a gradual diffusion of Ti into the ZnO. The XRD results also showed that broader peaks with a lower intensity were increasingly observed as a function of the milling time, to indicate that the average crystallite size decreased. The average crystallite size and lattice strain of the major phase were calculated by the Williamson–Hall equation [20]:

$$\frac{\beta\cos\theta}{\lambda} = \frac{0.9}{d} + \frac{\eta\sin\theta}{\lambda} \quad (1)$$

where β is the full width at the half maximum of the diffraction peak, θ is the Bragg angle, λ is the wavelength of X-ray used, d is an average crystallite size and η is a lattice strain. The results are displayed in Fig. 2.

The lattice strain increased when the milling time was increased to 10 h. Generally, a high-energy impact produces a vast amount of lattice imperfections, giving rise to a peak broadening. Thus, it could be said that dislocations, vacancies, interstitials, substitutionals and other defects such as stacking faults and twins lead to the formation of lattice strain [21]. As the milling time increased, the lattice imperfections increased and thus the lattice strain also increased. Nevertheless, the lattice strain decreased again if the milling time was further increased to 20 h. This reduction of the lattice strain can be attributed to an

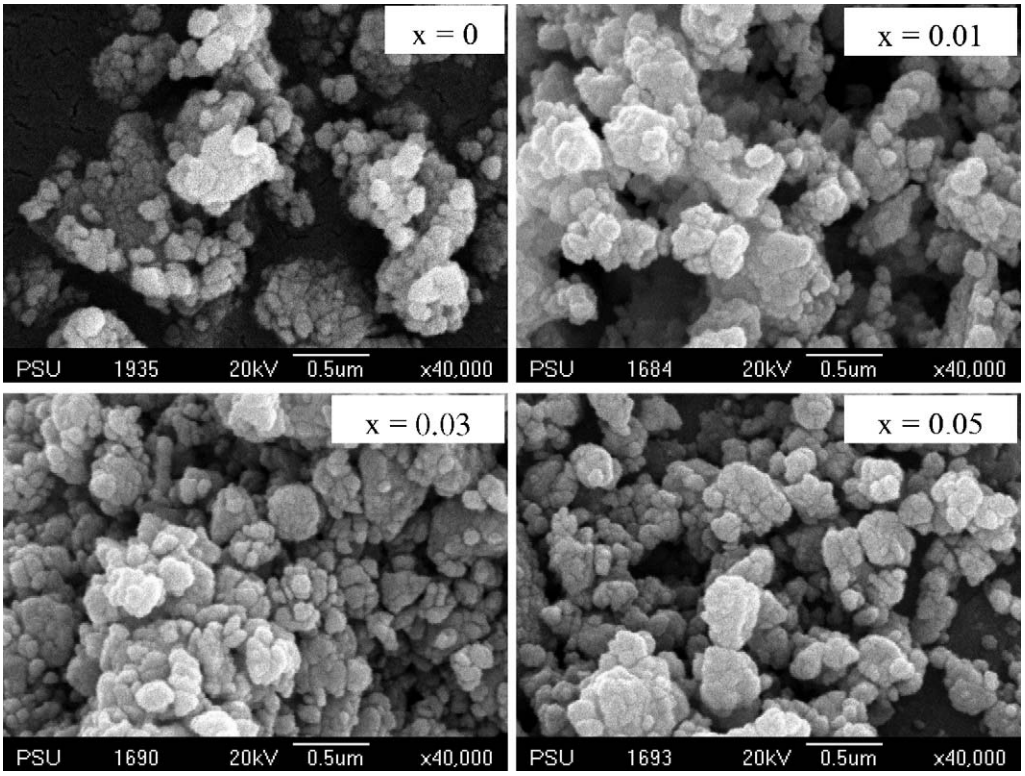

Fig. 5. SEM images of Ti-doped ZnO nanoparticles.

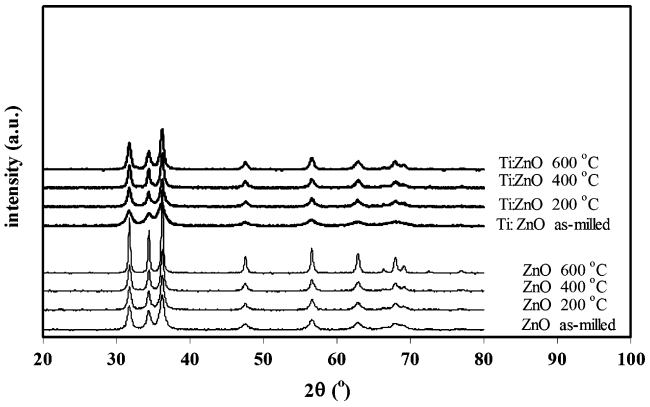

Fig. 6. XRD patterns of ZnO and $Zn_{0.95}Ti_{0.05}O$ nanoparticles at different annealing temperatures.

increase of temperature during prolonged milling [22]. A variation of crystallite size with milling time occurred as the inverse to the lattice strain. A dramatic decrease in crystallite size was obvious when the milling time was increased to 10 h because the mixtures became more fractured as a function of the milling time during the period of 1–10 h as a result of collisions between the powders and the milling media. In this study, a further increase of milling time to 20 h caused the crystallite size to increase. This is because the temperature rises during the milling, as a result of the kinetic energy of the grinding medium or the exothermic reaction during the milling process [22].

3.2. Effect of Ti doping content

The XRD patterns of as-prepared Ti-doped ZnO powders milled for 20 h are shown in Fig. 3.

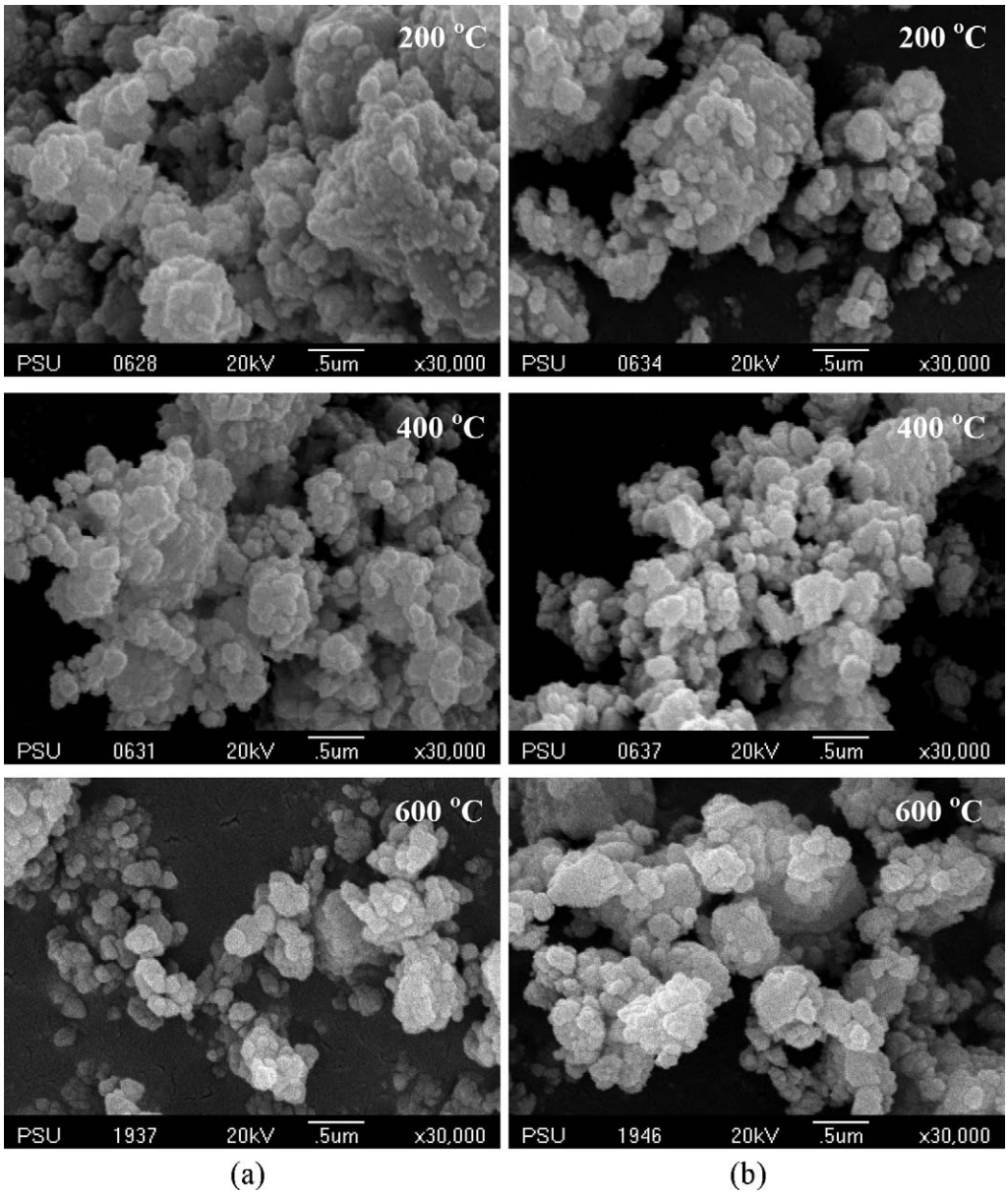

Fig. 7. SEM images of ZnO and $Zn_{0.95}Ti_{0.05}O$ nanoparticles at different annealing temperatures.

Table 1
Information on the properties of ZnO and $Zn_{0.95}Ti_{0.05}O$ nanoparticles.

Doping content (x)	Temperature (°C)	Crystallite size (nm)	Lattice strain	E_g (eV)	E_0
0	As-milled	22.1	1.36	2.96	0.33
	200	32.6	0.81	3.11	0.25
	400	35.9	0.73	3.12	0.23
	600	37.1	0.65	3.14	0.19
0.05	As-milled	17.6	1.03	3.01	0.33
	200	29.8	0.99	3.12	0.29
	400	32.5	0.82	3.13	0.20
	600	32.7	0.66	3.14	0.19

Wider diffraction peaks were observed as a higher Ti doping content was used. This indicates that a smaller crystallite size was formed. To confirm this, the crystallite size calculated by the Scherrer's equation [1] is presented in Fig. 4.

From Fig. 4, the calculated crystallite size corresponded to the peak broadening in Fig. 3. This is because the radius of Ti^{4+} (61 pm) is smaller than that of Zn^{2+} (74 pm) hence indicating a more complete incorporation of Ti^{4+} into the ZnO. The as-milled Ti-doped ZnO powders were further investigated by the SEM technique and the results are presented in Fig. 5.

The morphological characteristic of the Ti-doped ZnO nanoparticles with various Ti doping contents is similar for all cases. In this study, the primary spherical nanoparticles are agglomerated and the size of the spherical nanoparticle shows little change as a function of the Ti doping content.

3.3. Effect of annealing temperature

In this section, ZnO and $Zn_{0.95}Ti_{0.05}O$ nanoparticles were annealed in air at different temperatures and the XRD patterns of annealed powders are shown in Fig. 6. Upon annealing, the peak intensity improved and the full width at a half maximum decreased as the annealing temperature increased. This result indicated that the crystallinity of annealed ZnO and $Zn_{0.95}Ti_{0.05}O$ nanoparticles was improved as a function of the annealing temperature (Table 1).

The crystallite size calculated using the Scherrer's equation increased significantly when the annealing temperature was increased. In addition, the lattice strain was reduced when the crystallite size increased. This results from the reduction of defect concentration in ZnO and structural relaxation.

In this study, the grain growth can be explained by the following equation [23–24]:

$$D^n - D_0^n = Kt \tag{2}$$

where D is an average grain size at time t, D_0 is an average initial grain size, n is a grain-growth exponent depending on the growth mechanism and K is a constant that could be expressed by the following relationship.

$$K = K_0 \exp\left(-\frac{Q}{RT}\right) \tag{3}$$

where Q is the activation energy required for growth, K_0 is a constant, R is the gas constant and T is the absolute temperature. Considering the equations above, the crystallite size was further improved when the annealing temperature was increased.

Regarding the SEM images in Fig. 7, the particle size slightly increased as a function of annealing temperature and this is in good agreement with the crystallite size estimated using the Scherrer's equation.

3.4. Optical properties

In this part, the absorbance and band-gap values of ZnO and $Zn_{0.95}Ti_{0.05}O$ nanoparticles that prepared at different annealing temperatures were evaluated as a function of the wavelength

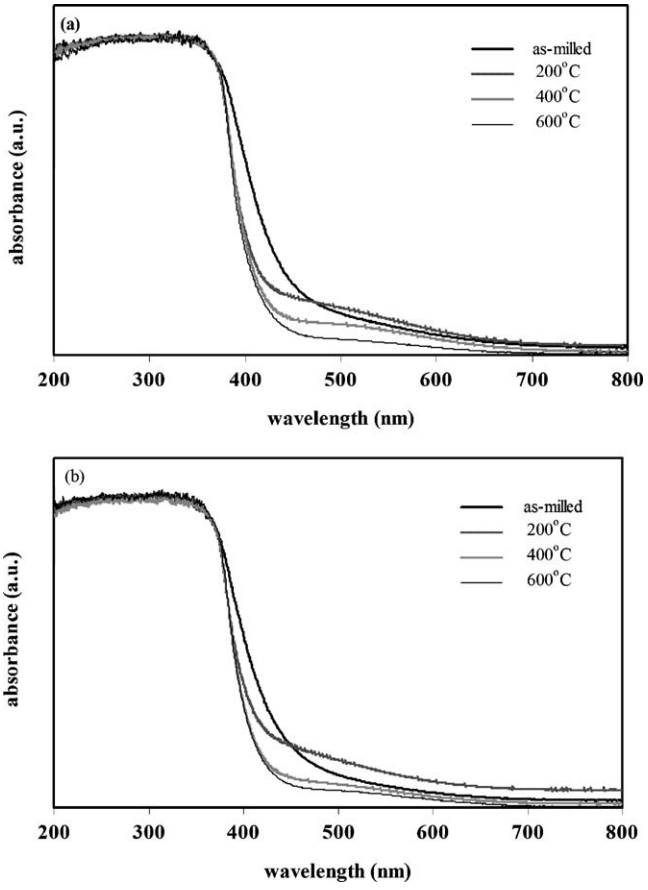

Fig. 8. The absorbance of as-milled and annealed samples at different temperatures. (a) ZnO and (b) $Zn_{0.95}Ti_{0.05}O$ nanoparticles.

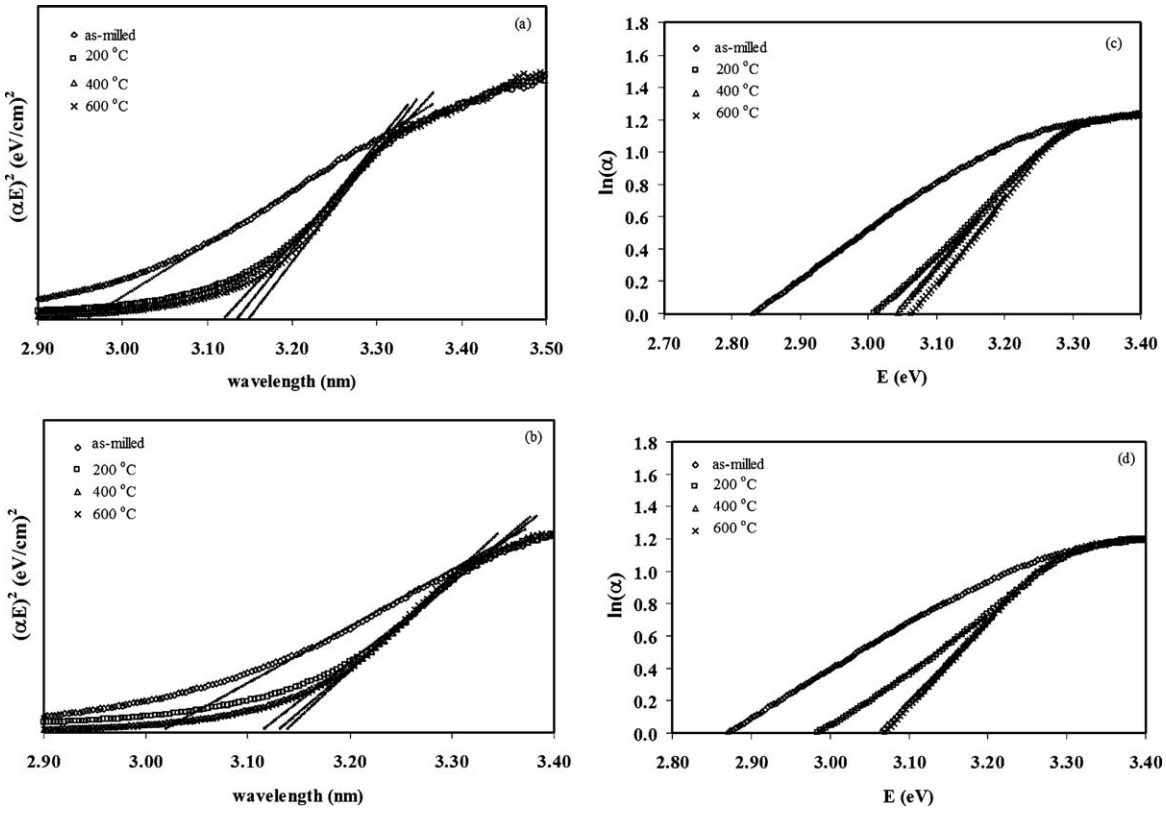

Fig. 9. Plots of $(\alpha E)^2$ versus E of as-milled and annealed samples at different temperatures (a) ZnO and (b) $Zn_{0.95}Ti_{0.05}O$ nanoparticles as well as the plots of $\ln(\alpha)$ versus E of as-milled and annealed samples at different temperatures (c) ZnO and (d) $Zn_{0.95}Ti_{0.05}O$ nanoparticles.

and the results are shown in Fig. 8. The samples were highly transparent in the visible region. The absorption edge shifted to a lower wavelength when the annealing temperature was increased. This indicated that the band-gap was wider as a function of the annealing temperature.

As shown in Fig. 9(a) and (b), the E_g values were estimated from a linear portion of the $(\alpha E)^2$ versus E curves using the following equations:

$$(\alpha E)^2 = E_D(E - E_g) \tag{4}$$

where E is the photon energy, E_g is the optical band-gap, E_D is a constant and α is an absorption coefficient that could be approximated by

$$\alpha = \frac{A}{d} \tag{5}$$

where A is the measured absorbance and d is the thickness of the cell. The E_g values of the samples at different annealing temperatures are given in Table 1. It is noteworthy that the E_g values increased when the crystallite size increased. It is well-known that the ZnO is an n-type semiconductor with a wide band-gap energy of about 3.2 eV [1,6], and the higher E_g value is usually achieved from the sample having a smaller crystallite size. In contrast, in this study, the higher E_g value of the annealed sample was obtained from samples having a larger crystallite size. Thus, it could be said that the E_g value of the sample occurred from an electronic transition between the valences states to the energy level of the generated defects within a forbidden band instead of an electronic transition between the filled valence bands to the empty conduction bands as is usual. This result can be confirmed by the reduction of the lattice strain and the concentration of defects (E_0) as shown in Table 1. The defects, for example oxygen vacancies, oxygen interstitials and zinc interstitials normally generated in ZnO crystals. These defects affect the optical properties as revealed in a few reports [25–27]. To confirm the influence of the defect concentration on the E_g value, the curves of $\ln(\alpha)$ versus E were plotted (Fig. 9c and d). The reciprocal values of the slopes from the linear part signify the defect concentration (E_0) and the results are shown in Table 1. Therefore, the E_g value can be increased by reducing the defect concentration.

Considering the effect of the Ti dopant on the E_g value at the same annealing temperature, the E_g value of $Zn_{0.95}Ti_{0.05}O$ nanoparticles was larger than that of the E_g value of undoped

Table 2
The effect of nanocrystalline ZnO and $Zn_{0.95}Ti_{0.05}O$ nanoparticles on the inhibition of various bacteria using an agar well diffusion method.

Doping content (x)	Inhibition zone diameter (mm)				
	S. aureus	*E. coli*	*P. mirabilis*	*S. typhi*	*P. aeruginosa*
0	15	11	13	16	20
0.05	15	13	12	14	18

ZnO powders. From Table 1, the crystallite size of $Zn_{0.95}Ti_{0.05}O$ nanoparticles was smaller than that of undoped ZnO powders as well as the defect concentration is similar at each annealing temperature. Thus the increase of E_g values for the Ti-doped ZnO powders can be explained by the reduction of the crystallite size [1].

3.5. Antibacterial activity

In this study, the antibacterial activity of as-milled ZnO and as-milled $Zn_{0.95}Ti_{0.05}O$ suspensions towards *S. aureus*, *E. coli*, *P. mirabilis*, *S. typhi* and *P. aeruginosa* was tested by an agar well diffusion method (Table 2).

It is evident that both as-milled ZnO and as-milled $Zn_{0.95}Ti_{0.05}O$ nanoparticles can damage both the Gram-positive bacteria (*S. aureus*) and Gram-negative bacteria (*E. coli*, *P. mirabilis*, *S. typhi* and *P. aeruginosa*). Under the conditions used, these tests were incubated in the dark. Therefore, the penetration of the particles into the cell wall is a mechanism to damage the bacteria [28].

4. Conclusions

$Zn_{1-x}Ti_xO$ (x = 0, 0.01, 0.03 and 0.05) nanoparticles with a hexagonal structure were successfully synthesized using a high-energy ball milling technique. The crystallite size decreased from 41.1 to 30.7 and 16.3 nm when the milling times were 1, 5 and 10 h, respectively. A further increase of the milling time to 20 h produced a slight increase in the crystallite size to 17.6 nm. In contrast, the strain changed inversely to the crystallite size. The crystallite size also increased as the annealing temperature increased. The optical band-gap of the sample was improved by doping with Ti and increasing the annealing temperature. The increase of the band-gap with the increase of annealing temperature can be explained by a reduction of the defect concentration. The as-milled samples can reduce the growth *S. aureus*, *E. coli*, *P. mirabilis*, *S. typhi* and *P. aeruginosa*.

Acknowledgements

The authors would like to acknowledge the financial support from the Research, Development and Engineering (RD&E) fund through The National Nanotechnology Center (NANOTEC), The National Science and Technology Development Agency (NSTDA), Thailand (Project No. NN-B-22-FN8-19-52-21) to Prince of Songkla University and the Center for Innovation in Chemistry (PERCH-CIC), Commission on Higher Education, Ministry of Education. The authors would like to acknowledge Dr. Brian Hodgson for English corrections.

References

[1] S. Suwanboon, P. Amornpitoksuk, A. Haidoux, J.C. Tedenac, Structural and optical properties of undoped and aluminium doped zinc oxide nanoparticles via precipitation method at low temperature, J. Alloys Compd. 462 (2008) 335–339.
[2] A. Moballegh, H.R. Shahverdi, R. Aghababazadeh, A.R. Mirhabibi, ZnO nanoparticles obtained by mechanochemical technique and the optical properties, Surf. Sci. 601 (2007) 2850–2854.
[3] A. Dodd, A. McKinley, T. Tsuzuki, M. Saunders, Tailoring the photocatalytic activity of nanoparticulate zinc oxide by transition metal oxide doping, Mater. Chem. Phys. 114 (2009) 382–386.
[4] C.Y. Hsu, C.H. Tsang, Effects of ZnO buffer layer on the optoelectronic performances of GZO films, Sol. Energy Mater. Sols. Cells 92 (2008) 530–536.
[5] L. Zhang, Y. Ding, M. Povey, D. York, ZnO nanofluids—a potential antibacterial agent, Prog. Nat. Sci. 18 (2008) 939–944.
[6] S. Suwanboon, Structural and optical properties of nanocrystalline ZnO powder from sol–gel method, Science Asia 34 (2008) 31–34.
[7] N. Samaele, P. Amornpitoksuk, S. Suwanboon, Morphology and optical properties of ZnO particles modified by diblock copolymer, Mater. Lett. 64 (2010) 500–502.
[8] B. Wang, C. Xia, J. Iqbal, N. Tang, Z. Sun, Y. Lu, L. Wu, Influences of Co doping on the structural, optical and magnetic properties of ZnO nanorods synthesized by hydrothermal route, Solid State Sci. 11 (2009) 1419–1422.
[9] Y.L. Chang, Y.H. Chang, I.G. Chen, G.J. Chen, Y.L. Chai, T.H. Fang, S. Wu, Synthesis, formation and characterization of $ZnTiO_3$ ceramics, Ceram. Int. 30 (2004) 2183–2189.
[10] A.M. Glushenkov, H.Z. Zhang, Y. Chen, Anomalous evaporation behavior of ZnO powder milled mechanically under high-energy conditions, Mater. Lett. 62 (2008) 715–718.
[11] K. Vojisavljevic, M. Scepanovic, T. Sreckovic, M. Grujic-Brojcin, Z. Brankovic, G. Brankovic, Structural characterization of mechanically milled ZnO: influence of zirconia milling media, J. Phys.: Condens. Matter. 20 (2008) 475202.
[12] L.C. Damonte, M.A. Hernandez-Fenollosa, M. Meyer, L. Mendoza-Zelis, B. Mari, Structural and magnetic properties in mechanically alloyed $Zn_{1-x}Co_xO$ semiconductor powders, Physica B 398 (2007) 380–384.
[13] L.C. Damonte, M.A. Hernandez-Fenollosa, B. Mari, Cation substitution in ZnO obtained by mechanical milling, J. Alloys Compd. 434–435 (2007) 813–815.
[14] Z.V. Marinkovic, L. Mancic, P. Vulic, O. Milosevic, Microstructural characterization of mechanically activated ZnO–Cr_2O_3 system, J. Eur. Ceram. Soc. 25 (2005) 2081–2084.
[15] S.K. Manik, S.K. Pradhan, Preparation of nanocrystalline microwave dielectric Zn_2TiO_4 and $ZnTiO_3$ mixture and X-ray microstructure characterization by Rietveld method, Physica E 33 (2006) 69–76.
[16] S.K. Manik, P. Bose, S.K. Pradhan, Microstructure characterization and phase transition kinetics of ball-milled prepared nanocrystalline Zn_2TiO_4 by Rietveld method, Mater. Chem. Phys. 82 (2003) 837–847.
[17] N. Obradovic, N. Mitrovic, V. Pavlovic, Structural and electrical properties of sintered zinc–titanate ceramics, Ceram. Int. 35 (2009) 35–37.
[18] N. Labus, N. Obradovic, T. Sreckovic, V. Mitic, M.M. Ristic, Influence of mechanical activation on synthesis of zinc metatitanate, Sci. Sinter. 37 (2005) 115–122.
[19] N. Obradovic, N. Labus, T. Sreckovic, D. Mitic, M.M. Ristic, Synthesis and characterization of zinc titanate nano-crystal powders obtained by mechanical activation, Sci. Sinter. 37 (2005) 123–129.
[20] P. Amornpitoksuk, S. Suwanboon, Correlation of milling time on formation of TiCoSb phase by mechanical alloying, J. Alloys Compd. 462 (2008) 267–270.
[21] S.B. Waje, M. Hashim, W.D.W. Yusoff, Z. Abbas, X-ray diffraction studies on crystallite size of $CoFe_2O_4$ nanoparticles prepared using mechanical alloying and sintering, Appl. Surf. Sci. 256 (2010) 3122–3127.
[22] M. Delshad Chermahini, M. Zandrahimi, H. Shokrollahi, S. Sharafi, The effect of milling time and composition on microstructural and magnetic properties of nanostructured Fe–Co alloys, J. Alloys Compd. 477 (2009) 45–50.
[23] M. Kambara, K. Uenishi, K.F. Kobayashi, Nano-structured intermetallic compound TiAl obtained by crystallization of mechanically alloyed amorphous TiAl, and its subsequent grain growth, J. Mater. Sci. 35 (2000) 2897–2905.
[24] Y. Caglar, S. Ilican, M. Caglar, F. Yakuphanoglu, J. Wu, K. Gao, P. Lu, D. Xue, Influence of heat treatment on the nanocrystalline structure of ZnO film deposited on p-Si, J. Alloys Compd. 481 (2009) 885–889.

[25] B. Ha, H. Ham, C.J. Lee, Photoluminescence of ZnO nanowires dependent on O_2 and Ar annealing, J. Phys. Chem. Solids 69 (2008) 2453–2456.
[26] S. Sepulveda-Guzman, B. Reeja-Jayan, E.D.L. Rosa, A. Torres-Castro, V. Gonzalez-Gonzalez, M. Jose-Yacaman, Synthesis of assembled ZnO structures by precipitation method in aqueous media, Mater. Chem. Phys. 115 (2009) 172–178.
[27] S. Dutta, S. Chattopadhyay, A. Sarkar, M. Chakrabarti, D. Sanyal, D. Jana, Role of defects in tailoring structural, electrical and optical properties of ZnO, Prog. Mater. Sci. 54 (2009) 89–136.
[28] L. Zhang, Y. Jiang, Y. Ding, M. Povey, D. York, Investigation into the antibacterial behaviour of suspensions of ZnO nanoparticles (ZnO nanofluids), J. Nanopart. Res. 9 (2007) 479–489.